Science of the Total Environment 1006 (2025) 180850

Contents lists available at ScienceDirect

Science of the Total Environment

journal homepage: www.elsevier.com/locate/scitotenv

Long-range transport of short-lived nitrogen dioxide in East Asia

Seung-Hee Baek [a], Hyo-Jung Lee [a,b,*], Hyun-Young Jo [c], Cheol-Hee Kim [a,b], Min-Jun Park [a], Jong-Min Kim [a], Juseon Bak [b], Hanlim Lee [d], Yeonjin Jung [d], Junsung Park [e], Jung-Hun Woo [f], Jinseok Kim [g,h], Rokjin Park [i], Lim-Seok Chang [j], Chang-Keun Song [k]

[a] Department of Atmospheric Science, Pusan National University, Busan, 46241, Republic of Korea
[b] Institute of Environmental Studies, Pusan National University, Busan, 46241, Republic of Korea
[c] Changwon Research Institute, Changwon, 51500, Republic of Korea
[d] Major of Spatial Information Engineering, Division of Earth Environmental System Science, Pukyong National University, Busan, 48513, Republic of Korea
[e] Atomic and Molecular Physics Division, Center for Astrophysics|Harvard & Smithsonian, Cambridge, MA, 02138, USA
[f] Graduate School of Environmental Studies, Seoul National University, Seoul, 08826, Republic of Korea
[g] Department of Advanced Technology Fusion, Konkuk University, Seoul, 05029, Republic of Korea
[h] Environmental Planning Institution, Seoul National University, Seoul, 08826, Republic of Korea
[i] School of Earth and Environmental Sciences, Seoul National University, Seoul, 08826, Republic of Korea
[j] Environmental Satellite Center, National Institute of Environmental Research, Incheon, 22689, Republic of Korea
[k] Department of Urban and Environmental Engineering, Ulsan National Institute of Science and Technology, Ulsan, 44919, Republic of Korea

HIGHLIGHTS

- Analyzed long-range transport of NO_2 over East Asia using satellite and WRF-Chem
- Wintertime NO_x lifetime of 1–3 days enables significant long-range transport.
- Strong winter westerlies drive NO_2 transport across the Yellow Sea to Korea Peninsula.
- FLEXPART-WRF simulations reveal seasonal shifts in transboundary pollutant pathways.

GRAPHICAL ABSTRACT

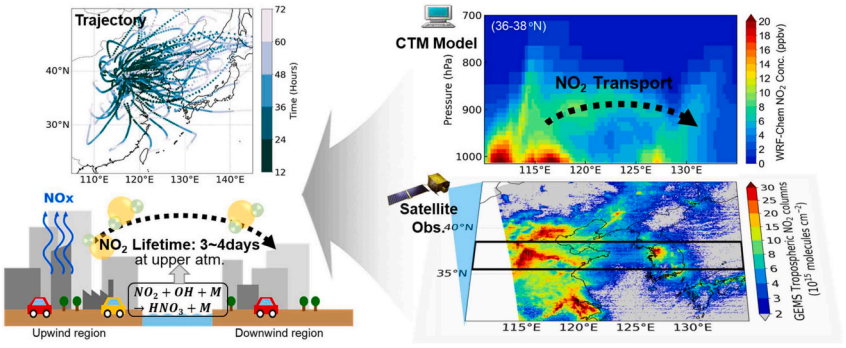

ARTICLE INFO

Keywords:
NO_2 transport
Short-lived climate pollutant
GEMS
WRF-Chem
Tropospheric NO_2 column
NO_x lifetime

ABSTRACT

This study explores the broader spatial influence of nitrogen dioxide (NO_2) over East Asia by integrating satellite and aircraft observations with chemical transport and trajectory model analyses. Tropospheric NO_2 column densities observed by the TROPOspheric Monitoring Instrument (TROPOMI) over the Yellow Sea—located between China and South Korea—are found to be 3.2 times higher in winter than the annual average, highlighting the role of prevailing westerlies in facilitating regional-scale transport during the cold season. Additional insights into the diurnal dynamics of NO_2 transport are provided by hourly observations from the Geostationary Environment Monitoring Spectrometer (GEMS). To further examine the mechanisms responsible for this transport,

* Corresponding author at: Department of Atmospheric Sciences, Pusan National University, 2, Busandaehak-ro 63beon-gil, Geumjeong-gu, Busan, 46241, Republic of Korea.
E-mail address: hyojung@pusan.ac.kr (H.-J. Lee).

https://doi.org/10.1016/j.scitotenv.2025.180850
Received 8 July 2025; Received in revised form 29 September 2025; Accepted 29 October 2025
Available online 11 November 2025

satellite-based evidence is complemented by in situ aircraft measurements and chemical transport model simulations. Aircraft profiles over the Yellow Sea confirm that NO_2 can be extensively transported at altitudes of 1–2 km under favorable meteorological conditions. Model results indicate that the lifetime of NO_x in major urban areas—such as the Beijing–Tianjin–Hebei region and the Seoul Metropolitan Area—can be extended from several hours to 1–3 days, depending on meteorological conditions. Trajectory analyses further suggest that NO_x originating from East Asia can reach downwind regions across adjacent seas within 12–24 h. These findings underscore the importance of accounting for the long-range transport of short-lived pollutants in the development of national air quality management strategies.

1. Introduction

The increase in anthropogenic pollutant emissions has significantly contributed to global air quality degradation, with East Asia emerging as a particularly critical region due to rapid industrialization and urbanization. Consequently, emissions of air pollutants from East Asia and their long-range transport across national and continental boundaries have become a major focus of scientific research (Carmichael et al., 2002; Lee et al., 2019; Qu et al., 2016). While most studies on long-range transport have concentrated on pollutants with relatively long atmospheric lifetimes, such as carbon monoxide (CO), particulate matter (PM), and ozone (O_3) (Cooper et al., 2011; Liang et al., 2004; Parrish et al., 2004), the role of nitrogen oxides (NO_x) has gained increasing attention in recent years.

NO_x, including nitrogen monoxide (NO) and nitrogen dioxide (NO_2), are primarily emitted from anthropogenic sources such as transportation, industrial processes, power plants, and fossil fuel and biomass combustion (Jaeglé et al., 2005; van der A et al., 2008). These oxides serve as key precursors of secondary harmful pollutants, including tropospheric O_3 and nitrate aerosols (Bassett and Seinfeld, 1983; Crutzen, 1970; Kang et al., 2020; Wang et al., 2011). During transport, the chemical transformations of nitrate species significantly impact air quality in downwind regions (Derwent and Nodopt, 1986; Lee et al., 2022; Uno et al., 2017; Zhang et al., 2008). Despite their relatively short atmospheric residence time—typically less than one day (Granier and Brasseur, 2003; Leue et al., 2001)—the lifetime of NO_x varies considerably depending on environmental factors such as region and season. Within the boundary layer, NO_x lifetime ranges from approximately 6 h in summer to 12–20 h in winter, influenced by changes in atmospheric photolysis rates and water vapor content (Lamsal et al., 2010; Martin et al., 2003; Shah et al., 2020). In the upper troposphere, NO_x exhibits a longer lifetime of 5–10 days, allowing sufficient time for long-range transport (Jaeglé et al., 1998; Stohl et al., 2002). These spatiotemporal variations in NO_x lifetime critically determine its horizontal and vertical distributions, influencing its potential for long-range transport (Lee et al., 2014; Li et al., 2023; Matandirotya and Burger, 2021; Schaub et al., 2005; Stohl et al., 2002; Wenig et al., 2003).

Among NO_x, NO_2 is particularly important for long-range transport studies due to its greater stability and longer atmospheric lifetime compared to NO. NO_2 is also well-suited for large-scale monitoring, as it can be precisely observed using advanced satellite and ground-based systems, such as the TROPOspheric Monitoring Instrument (TROPOMI) (Veefkind et al., 2012) and the Geostationary Environment Monitoring Spectrometer (GEMS) (Kim et al., 2020). These instruments provide high-resolution data on NO_2 distribution, making it a practical and scientifically meaningful focus for investigating pollutant transport across East Asia. Over the course of the past two to three decades, satellite sensors such as the Global Ozone Monitoring Experiment (GOME), SCanning Imaging Absorption SpectroMeter for Atmospheric CartograpHY (SCIAMACHY) (Bovensmann et al., 1999), Ozone Monitoring Instrument (OMI) (Levelt et al., 2018), GOME-2 series (Callies et al., 2000) and TROPOMI have provided valuable insights into global tropospheric NO_2 column distributions. Long-term analyses of these datasets have revealed consistent trends in NO_x emissions, with East Asia consistently exhibiting high NO_2 concentrations (Kim et al., 2006; Richter et al., 2005; Stavrakou et al., 2008; van der A et al., 2006, 2008; Zhang et al., 2007). These satellite measurements can provide information on high-emitting regions and are capable of capturing enhanced NO_2 columns over downwind areas, thereby offering insight into the long-range transport of gaseous nitrogen oxides.

In this study, we utilized data from state-of-the-art atmospheric monitoring technologies, including TROPOMI, GEMS, ground-based and aircraft measurements, as well as Weather Research and Forecasting model coupled with Chemistry (WRF-Chem) simulations, to investigate the long-range transport of NO_x through an integrated approach. Specifically, we analyzed the spatiotemporal characteristics of tropospheric NO_2 during its long-range transport and provide a numerical basis for the variability in NO_x lifetime. Our analysis encompassed the horizontal and vertical pathways of long-range NO_2 transport in East Asia, as observed during the Satellite Integrated Joint Monitoring of Air Quality (SIJAQ) 2021 field campaigns. The findings of this study are intended to contribute to ongoing regional air-quality management efforts and support policy decisions aimed at mitigating the health impacts associated with NO_2 pollution.

2. Materials and methods

2.1. Satellite observations

The TROPOMI, launched in October 2017, is a single payload aboard the European Space Agency (ESA)'s Sentinel-5 Precursor (S—5P) spacecraft (Lorente et al., 2021; Veefkind et al., 2012). It operates in a sun-synchronous orbit with an equatorial crossing local time of 13:30, providing 14 to 15 orbits and global coverage daily. The spatial resolution of initially 3.5×7 km^2 at nadir was increased on 6 August 2019 to 3.5×5.5 km^2 (van Geffen et al., 2019). In this study, we utilized multi-year TROPOMI NO_2 data primarily to investigate the long-term seasonal variability of tropospheric NO_2 across East Asia, thereby providing a climatological context for the episodic transport events.

The GEMS was launched into space in February 2020 on the Geostationary Korea Multi-Purpose Satellite-2B (GK-2B), together with Geostationary Ocean Color Imager (GOCI) -2 (Kim et al., 2020). In this study, GEMS observations play a pivotal role in diagnosing transboundary pathways with their continuous daytime hourly monitoring capability over Asia, covering 5–45°N latitude and 75–145°E longitude. The GEMS provides full-scan images at least eight times from early morning to late afternoon (e.g., 8 am to 5 pm in Korea), a spatial resolution of approximately 3.5×8 km^2 (Kim et al., 2020; Oak et al., 2024; Seo et al., 2025). Previous validation studies with Version 2.0 (V2.0) reported systematic seasonal biases, particularly an overestimation of NO_2 columns around local noon during winter and early spring at Northern Hemisphere midlatitudes (Bae et al., 2025). By contrast, V3.0 exhibits an improvement exceeding 20 % in regression slopes relative to TROPOMI (Lee et al., 2024). In this study, we utilized the V3.0 Level 2 NO_2 retrievals from GEMS at six observation times per day, corresponding to two high-concentration episodes (Table S1). The high temporal resolution of GEMS allowed us to capture and track the evolution of NO_2 plumes on an hourly basis during these transboundary events, providing unprecedented insight into their development and movement.

The principle of the retrieval methodology is highly similar between GEMS and TROPOMI, comprising spectral fitting, stratosphere-troposphere separation (STS), and Air Mass Factor (AMF) correction (SCD to VCD conversion). The differential optical absorption spectroscopy (DOAS) (Platt and Stutz, 2008) fitting is applied to derive NO_2 slant column density (SCD) from absorption signatures measured by GEMS (432–450 nm) (Lee et al., 2024) and TROPOMI (405–465 nm) (Griffin et al., 2019; van Geffen et al., 2019), which represents the total amount of NO_2 integrated along the line of sight. To distinguish between stratospheric and tropospheric contributions to total SCDs, the stratospheric column is determined by summing the model-derived quantities above the tropopause. For GEMS, a priori NO_2 profiles are simulated from the Goddard Earth Observing System Chemistry model (GEOS-Chem), with the tropopause fixed at 230 hPa (Lee et al., 2024). For TROPOMI, the Tracer Model version 5 - Massively Parallel (TM5-MP) chemistry transport model and data assimilation system are used to determine both NO_2 profiles and the tropopause (van Geffen et al., 2019). The residual SCD, obtained by subtracting the stratospheric SCD from the total SCD, is finally converted into the tropospheric vertical column density (VCD) through AMF correction.

2.2. In situ observations during the SIJAQ 2021 campaign

The SIJAQ 2021 campaign was conducted from October 18 to November 25, 2021, focusing on the Seoul Metropolitan Area (SMA) and extending to broader regions across the Korean Peninsula. The campaign aimed to provide a comprehensive characterization of atmospheric composition, facilitating a detailed analysis of transboundary pollution and the impact of local emissions on regional air quality. To achieve these objectives, a multi-platform observational approach was adopted, integrating ground-based monitoring, airborne in situ measurements, satellite observations, and air-quality modeling, thereby ensuring robust analysis and cross-validation of results.

Ground-level measurements of NO_2 and fine particulate matter ($PM_{2.5}$) were obtained from the National Institute of Environmental Research (NIER) in South Korea and the China National Environmental Monitoring Center (CNEMC), with monitoring stations distributed across both countries (Fig. S1). Quality assurance (QA) and quality control (QC) procedures were implemented following the official regulations of the respective monitoring agencies. After further filtering to exclude missing or invalid values, the datasets formed the basis for identifying high-concentration episodes during SIJAQ 2021 and for evaluating the performance of the WRF-Chem model simulations.

In addition to ground-based monitoring, a total of 15 in situ aircraft flights were conducted during the campaign to characterize the vertical and horizontal distribution of air pollutants over the SMA and the Yellow Sea. These flights collected comprehensive measurements of trace gases and meteorological parameters, including NO_2, which was measured using a Teledyne API T500U analyzer (San Diego, CA, USA) based on cavity attenuated phase shift spectroscopy (measurement range: 40 pptv to 1000 ppbv, precision: 0.5 %). The campaign dataset was released after undergoing QA and QC procedures. In particular, missing values had already been excluded, and measurements below 250 m altitude during take-off and landing phases were not included in the dataset. Detailed information on the spatial and temporal coverage of the aircraft measurements is provided in Fig. 4 and Table S2. Collectively, these airborne and ground-based datasets served as a critical reference for interpreting satellite observations and for validating model-based analyses of transboundary pollution episodes.

2.3. WRF-Chem

The regional air-quality model employed in this study is WRF-Chem v3.9.1 (Skamarock et al., 2008). This model operates as an online system, wherein chemical and meteorological processes are integrated in real time (Grell et al., 2005). We specifically aimed to simulate NO_2 concentrations within East Asia, including the Korean Peninsula, China, and Japan, as shown in Fig. S1. The simulation domain was configured with a horizontal resolution of 27 × 27 km^2 and 28 sigma levels vertically. The National Centers for Environmental Prediction (NCEP) Final Analysis (FNL) data were used to establish the initial and boundary meteorological conditions, providing meteorological details at 1° × 1° horizontal resolution and updated every 6 h. The anthropogenic emissions dataset used to drive model is the updated Comprehensive Regional Emissions for Atmospheric Transport Experiment, version3 (CREATEv3). This dataset is based on a bottom-up emission inventory approach, which combines the Multiresolution Emission Inventory for China (MEIC) for China's emissions and the Clear Air Policy Support System (CAPSS) for Korea's emissions (Kim et al., 2023b). A detailed description of the emission inventory is documented in Woo et al. (2020). The chemical mechanisms incorporated in this study include the Regional Atmospheric Chemical Mechanism (RACM) and the Modal Aerosol Dynamics modeling for the Europe/Volatility Basis Set (MADE/VBS) scheme. These chemical options were selected to ensure a comprehensive depiction of the chemical transformations within the model. The physical and chemical processes integrated into the simulation are summarized in Table S3, offering a clear view of the model setup. The model performance was evaluated against observations of surface NO_2 showing generally good agreement ($R = 0.77–0.82$; Fig. S2). Simulation results were subsequently used to estimate the chemical lifetime of NO_x under various atmospheric conditions, providing quantitative insight into the persistence and transformation of NO_2 during long-range transport events across East Asia.

2.4. FLEXPART-WRF

The FLEXible PARTicle dispersion model (FLEXPART) is a Lagrangian particle dispersion model that has been extensively used to simulate atmospheric transport and dispersion processes on various scales (Brioude et al., 2013). It has been particularly applied to investigate the long-range transport of air pollutants and local pollution events (An et al., 2014; Brioude et al., 2013; Karmakar et al., 2022; Lee et al., 2014; Madala et al., 2015; Stohl et al., 2011). In this study, we employed FLEXPART-WRF v3.3 (Brioude et al., 2013), which operates in conjunction with the mesoscale meteorological model, WRF (Skamarock et al., 2008). The WRF simulations were conducted over East Asia, including the Korean Peninsula, China, and Japan, with a horizontal resolution of 27 × 27 km^2 and 30 vertical levels. The output fields were generated at an hourly temporal resolution. The FLEXPART-WRF simulations were performed at a horizontal resolution of 0.25° × 0.25° with 7 vertical layers spanning from 100 m to 5000 m. Forward simulations were conducted using air tracers with a three-day atmospheric lifetime to understand the seasonal transport and dispersion of air parcels. The simulations were performed for each season of 2021. Emissions were released within an altitude range of 50–2000 m. To assess how far air masses travel within three days, the model was executed in three-day segments throughout one month in each season of 2021. This setup provides a detailed representation of atmospheric dispersion and air mass transport pathways, enhancing understanding of pollutant movement and source-receptor relationships across the region. The FLEXPART-WRF simulations were specifically used to examine the seasonal trajectories of air parcels, revealing the primary directions and distances of pollutant transport for each season.

2.5. EDGAR v8.1 emission dataset

In this study, we used the Emissions Database for Global Atmospheric Research (EDGAR) version 8.1 Fast Track 2022 (FT2022) Air Pollutant (AP) emission dataset provided by the European Commission Joint Research Centre (JRC). This dataset reports monthly national total emissions of NO_x for the period 2000–2022, covering more than 200 countries worldwide. The total NO_x emissions include all anthropogenic

sectors: power generation, industrial combustion and processes, transportation (including road traffic, aviation, and shipping), residential and commercial combustion (including heating and cooking), agriculture, and waste. For this study, we extracted the EDGAR v8.1 FT2022 total NO_x emissions for South Korea, China, and Japan to investigate the long-term and seasonal variability of national-scale anthropogenic NO_x emissions.

3. Results and discussion

3.1. Climatological overview of NO_2 seasonality

Fig. 1 shows the monthly mean tropospheric NO_2 columns from the TROPOMI measurements for 2021–2023. The spatial distribution during the summertime (June–August) indicates that major urban centers, including the Beijing–Tianjin–Hebei (BTH) region and Shanghai in China, the SMA and Busan in South Korea, and Tokyo and Osaka in Japan, exhibit relatively high concentrations of tropospheric NO_2 (see Fig. S1 for a breakdown of each region). Satellite observations reveal a distinct seasonal variation in NO_2 column concentrations across East Asia, with peak values from winter to early spring reaching approximately 2.5 times the annual mean. A closer examination of seasonality in major cities shows that the BTH region in China; SMA in South Korea; Tokyo in Japan; and the Yellow Sea regions all experience a distinct seasonal variation with higher NO_2 concentrations in winter and lower concentrations in summer. Notably, NO_x emissions originating mainly from industrial and transportation sectors undergo little seasonal variation (Qu et al., 2016; Zhang et al., 2009), and anthropogenic NO_x emissions in China show limited seasonality, with a winter–summer ratio of 1.15 (Li et al., 2017; Zhang et al., 2007). The limited seasonality of NO_x emissions is further corroborated by Fig. 2, which demonstrates minor seasonal fluctuations in NO_x emissions. The observed seasonal patterns in NO_2 columns across East Asia, with maxima in winter and minima in summer, can be attributed to seasonal variations in NO_x lifetime. During the summer, NO_x has a shorter lifetime due to enhanced oxidation by hydroxyl radical (OH) in the daytime, significantly influencing afternoon NO_2 levels (Shah et al., 2020). In contrast, during winter, the NO_x lifetime within the boundary layer extends to approximately ~1 day, longer than in summer, supporting the hypothesis that NO_2 columns peak in winter (Beirle et al., 2003; Lee et al., 2014; Shah et al., 2020; van der A et al., 2006).

Therefore, over the Yellow Sea between China and the Korean Peninsula, the NO_2 column concentrations remain relatively low at ~1–3 × 10^{15} molecules cm^{-2} during summer but increases considerably by up to 5 × 10^{15} molecules cm^{-2} during winter. Furthermore, as shown in Figs. 1b and S3, pronounced springtime increase in NO_2 concentrations—absent in the three major cities of the BTH region—were broadly observed across downwind zones located within the latitude band influenced by prevailing westerlies. In particular, our analysis of observed-surface wind patterns in regions adjacent to the Yellow Sea further confirms the frequent occurrence of strong northwesterly and westerly winds during both spring and winter (Fig. S4). This pattern is consistent with previous studies that have identified the seasonal dominance of westerly-type winds over East Asia throughout the winter–spring period (Itahashi et al., 2017; Jung et al., 2022; Lee et al., 2014; Qu et al., 2016). Such meteorological conditions likely contribute to the elevated NO_2 concentrations observed in downwind regions, highlighting the critical role of seasonal wind patterns in pollutant transport. These findings are consistent with long-term OMI tropospheric NO_2 column data (2005–2020) (Lee et al., 2014), which exhibit a consistent seasonal pattern (Fig. S5). Our study aims to provide a comprehensive analysis of NO_2 long-range transport in East Asia, leveraging these seasonal characteristics observed in long-term measurements.

3.2. NO_2 long-range transport in cases with prevailing westerlies

Due to the measurement characteristics of polar-orbiting satellites, TROPOMI and OMI provide global NO_2 monitoring but they have limited capability for continuous hourly coverage of multiple weather or pollution events over short periods of time. South Korea's GEMS satellite offers hourly observations of the East Asian region but suffers from significant measurement data gaps. Ground-based measurements provide continuous monitoring; however, measurement gaps persist over regions such as the oceans. Consequently, additional measurements are needed to capture transboundary NO_2 transport events comprehensively. To investigate NO_2 behaviors over a large area in spring–winter under conditions favoring long-range transport, we employed intensive aircraft measurements over the Yellow Sea and integrated them with ground-based observations. As part of this, the aircraft measurements during the SIJAQ 2021 campaign were employed. We examined the long-range transport of pollutants from China driven by the prevailing westerlies, and compared it to atmospheric stagnation over the Korean Peninsula under high-pressure, low wind conditions. NO_2 behavior was analyzed under conditions conducive to pollutant transport (Fig. 3). Fig. 3a presents the 24-h average surface concentrations of $PM_{2.5}$ and NO_2 during the SIJAQ 2021 campaign. We classified the periods as long-range transport (LRT) and stagnation (STG) cases based on criteria established from various measurements and synoptic weather chart analyses conducted during the previous SIJAQ 2021 campaign (Kim et al., 2023a). The distinction between the two cases was further validated by satellite-derived AOD and model-simulated $PM_{2.5}$ distributions, which revealed clear spatial contrasts (Fig. S6). Under the influence of a migratory high, westerlies dominated the Shandong–Yellow Sea–Korea Peninsula region, facilitating the LRT of $PM_{2.5}$, with concentrations peaking at 97.32 μg m^{-3} in SMA on November 18–21; this event was designated an LRT case. In contrast, during October 25–28, air masses arriving from the ocean and the presence of northerly or easterly winds around SMA limited pollutant transport, resulting in a relatively low peak $PM_{2.5}$ concentration of 28.27 μg m^{-3}. This period was classified as an STG case. Maximum NO_2 concentrations in the LRT and STG cases were 45.33 and 40.87 ppbv, respectively, indicating no substantial difference. This can be attributed to the fact that NO_2 concentrations are not only influenced by long-range transport but also strongly affected by local emissions, making their transport-related signals less distinct compared to $PM_{2.5}$. Fig. 3b illustrates NO_2 concentrations and wind fields simulated by the WRF-Chem model for the LRT and STG periods. Comparative validation demonstrated strong agreement between model simulations and ground-based NO_2 observations in the SMA, with a correlation coefficient (R) of 0.77 and an index of agreement (IOA) of 0.86 (Fig. S2). Additionally, the WRF-Chem-derived tropospheric NO_2 column revealed that in the LRT case, NO_2 extended from China across the Yellow Sea along the westerlies, reaching the western coast of the Korean Peninsula—a pattern absent in the STG case. Spatiotemporal variations of the tropospheric NO_2 column, as observed by the GEMS satellite during both periods (Fig. 3c), indicated that during LRT events, concentrations exceeded 30 × 10^{15} molecules cm^{-2} over the BTH region in eastern China. The elevated NO_2 column was not confined to the BTH region but extended to adjacent areas such as the North China Plain and Shandong Province. Furthermore, in the LRT case, the NO_2 plume originating from China traversed the Yellow Sea, reaching concentrations of 3–6 × 10^{15} molecules cm^{-2} over both the Yellow Sea and Korean Peninsula. In contrast, during the STG case, high NO_2 concentrations persisted in known emission hotspots such as the BTH region, Shanghai, and the SMA, but NO_2 levels over the Yellow Sea remained below 2 × 10^{15} molecules cm^{-2}, with even lower concentrations along the coastline.

Satellite data typically provide column concentrations of pollutants in the atmosphere but do not offer detailed insight into their vertical distribution. To address this limitation and gain insight into the vertical distribution of long-range NO_2 transport, we combined aircraft

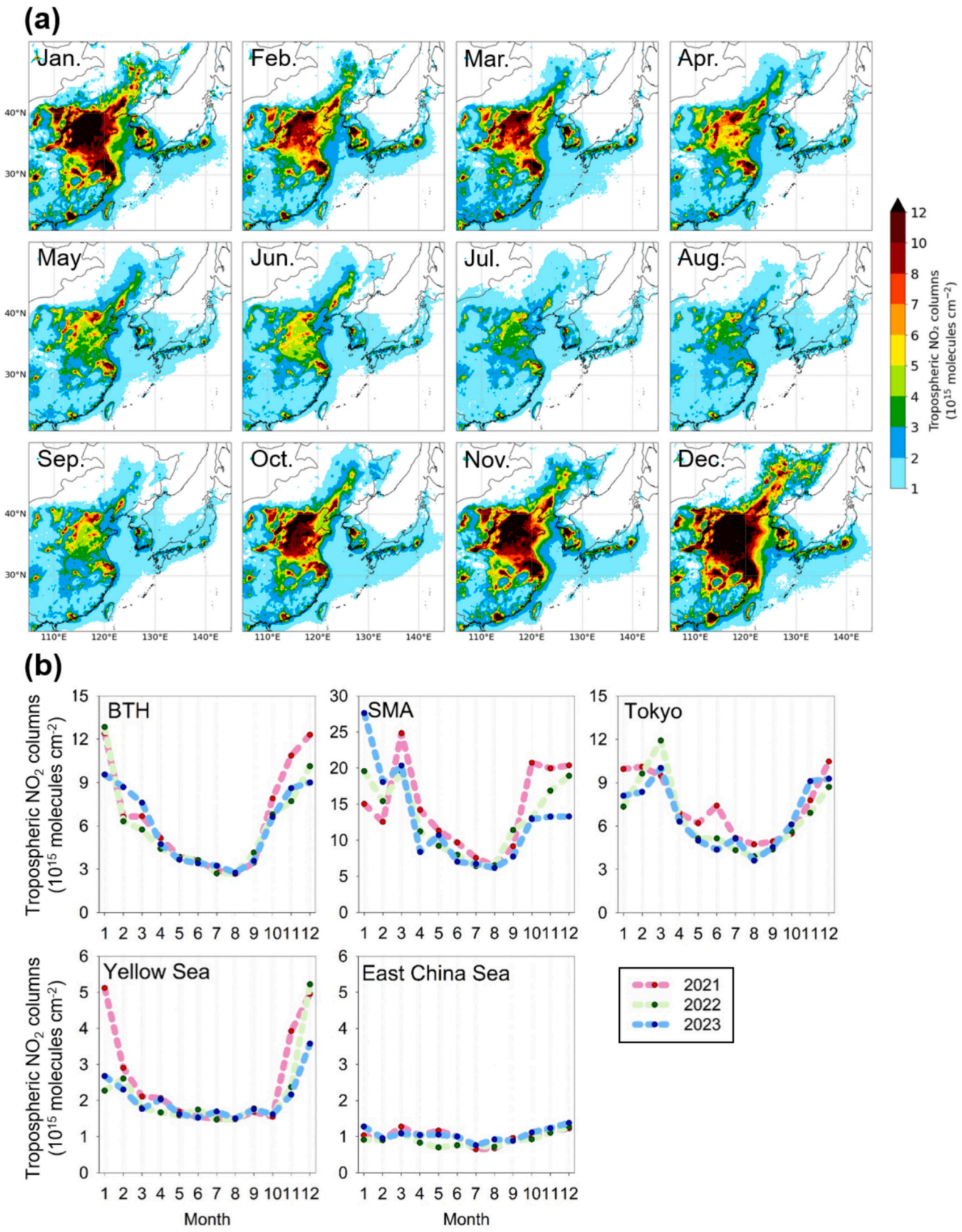

Fig. 1. Monthly tropospheric NO_2 column densities from TROPOMI over East Asia, with spatial distributions averaged over 2021–2023 (a) and monthly variations in selected regions (b).

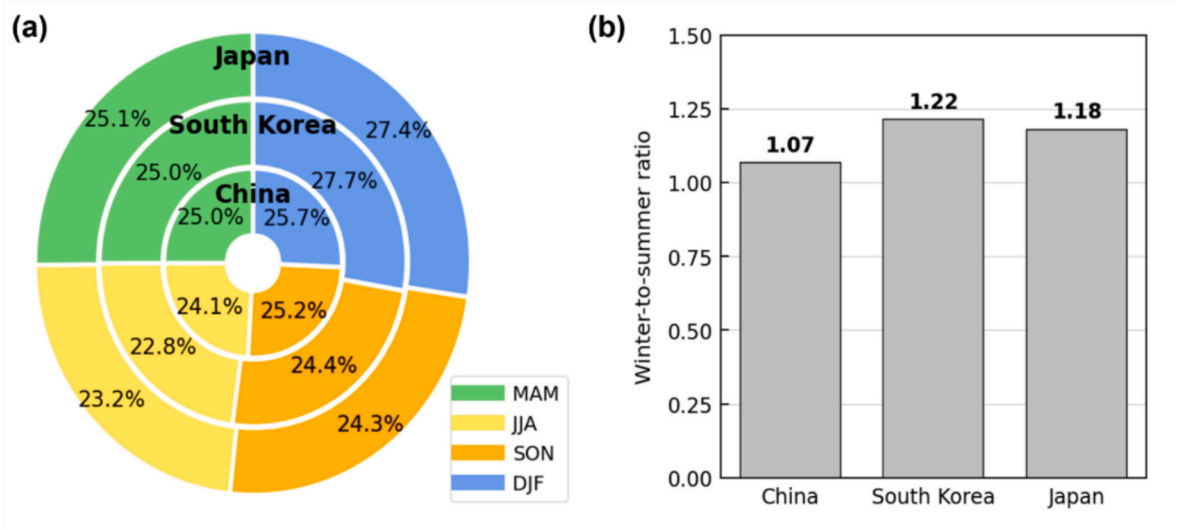

Fig. 2. Seasonal NO_x emissions and winter-to-summer ratios in China, South Korea, and Japan from 2000 to 2022 based on EDGAR v8.1 data.

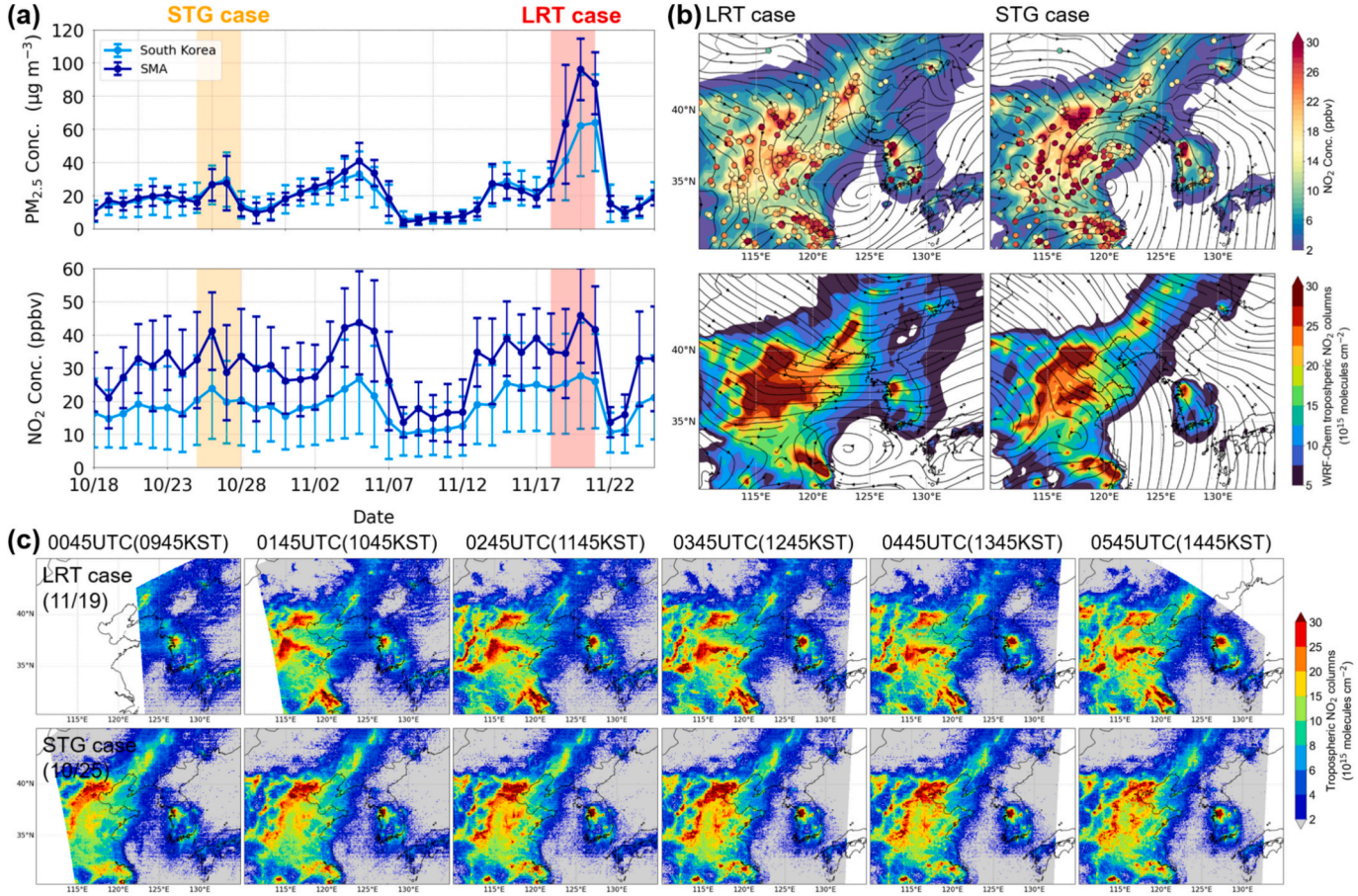

Fig. 3. Temporal and spatial distributions of NO_2 during LRT and STG cases, including time series of ground-level $PM_{2.5}$ and NO_2 over South Korea and SMA during the SIJAQ 2021 campaign (a), WRF-Chem-simulated surface (top) and tropospheric NO_2 (bottom), with wind streamlines at the surface (top) and the 850-hPa isobaric level (bottom) (b), and hourly GEMS-retrieved tropospheric NO_2 column densities on 19 November (LRT case) and 25 October (STG case) at six time points from 00:45 to 05:45 KST (09:45–14:45 UTC) (c).

measurements with air-quality model simulations. Fig. 4 presents the vertical NO_2 profiles obtained from aircraft measurements and WRF-Chem simulations during the LRT and STG periods. The STG case exhibited significantly lower NO_2 concentrations than the LRT case. Additionally, in the STG case, both aircraft measurements and model simulations demonstrated a decreasing concentration trend with increasing altitude. In contrast, during the LRT case, the model tended to underestimate NO_2 concentrations compared to measurements, although the vertical profile shapes remained similar. Notably, a concentration peak appeared at an altitude of 0.5–1.5 km over the Yellow

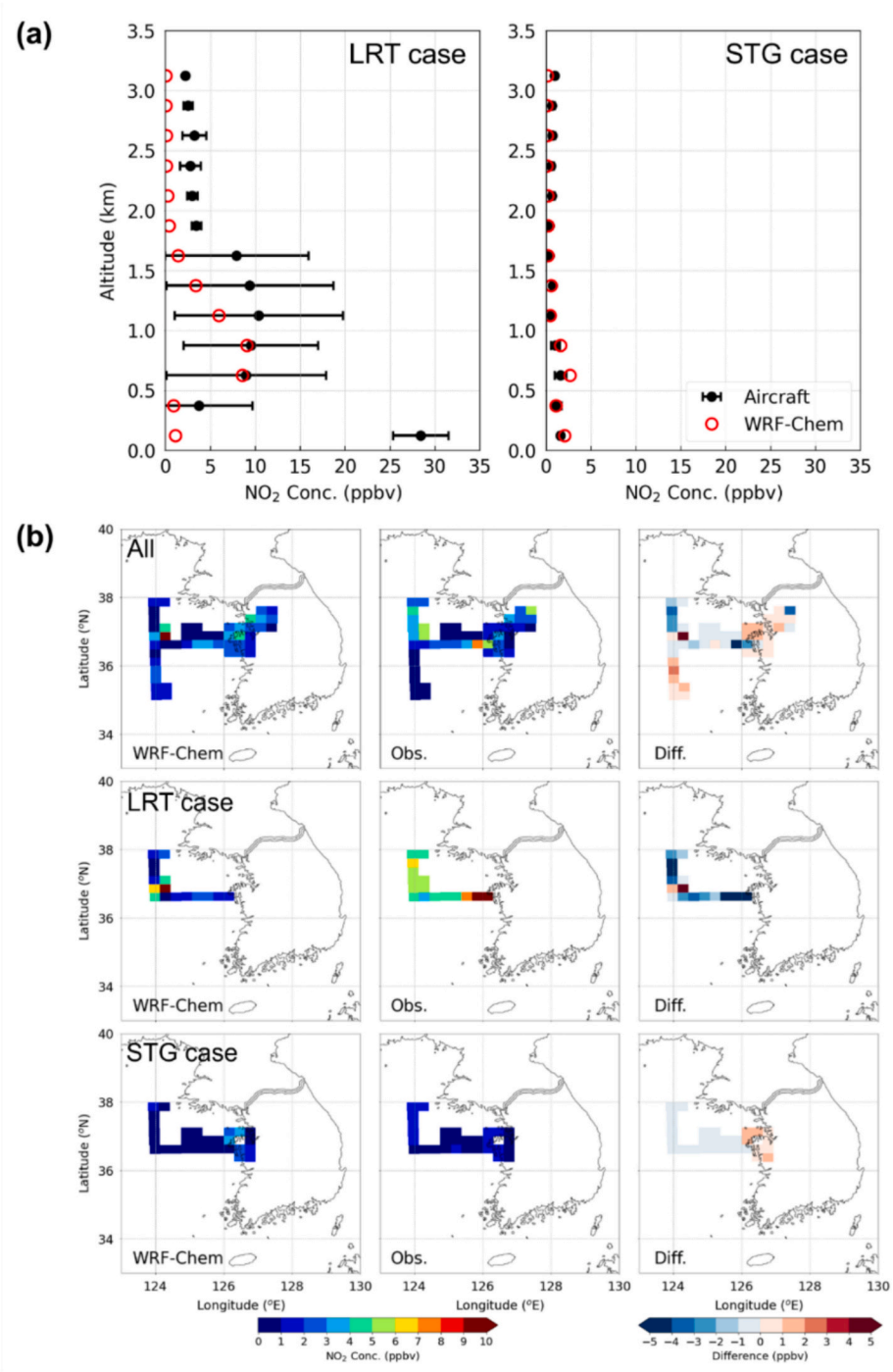

Fig. 4. Vertical distributions of NO_2 from aircraft measurements and WRF-Chem simulations during the SIJAQ 2021 campaign, sampled at aircraft measurement times (a), and comparisons along research flight paths mapped to the WRF-Chem model grid (b) (see Table S2 for details).

Sea. The WRF-Chem simulation of the NO_2 distribution at the 850-hPa isobaric level (corresponding to 1.5 km altitude) in Fig. 5 further indicates that the BTH–Shandong–Yellow Sea region is connected by a high-concentration NO_2 band in the LRT case, a structure absent in the STG case. Long-range transport of other long-lived air pollutants predominantly occurs at altitudes between 1 and 1.5 km (Ge et al., 2022; Guerova et al., 2006; Thomas and Devasthale, 2017; Thompson et al., 2019). Our findings suggest that NO_2 can also undergo transboundary transport at this altitude, albeit in relatively smaller amounts compared to other long-lived pollutants.

3.3. *Spatiotemporal variations in NO_x lifetime*

The LRT of NO_2 is determined by its atmospheric lifetime and the advective speed of the air mass. The NO_x lifetime is defined as the duration during which emitted NO_x undergoes chemical processes, such as O_3 production. This lifetime depends on the chemical environment, particularly the concentration of NO_x (Cooper et al., 2017; Duncan et al., 2013; Gu et al., 2016; Lamsal et al., 2011; Lu and Streets, 2012; Laughner and Cohen, 2019; Stavrakou et al., 2008; Valin et al., 2011). Laughner and Cohen (2019) reported a range of theoretically calculated NO_x lifetimes under the assumption of a steady-state HO_x family,

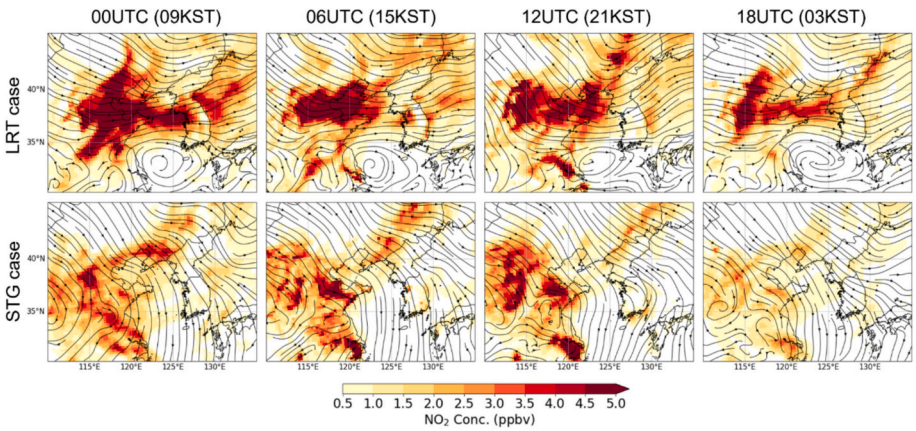

Fig. 5. Spatial distributions of NO_2 concentrations with 850-hPa wind streamlines from WRF-Chem simulations during high-concentration cases, shown at 6-h intervals (00, 06, 12, and 18 UTC).

demonstrating that in regions with significant NO_x emissions, the lifetime increases with NO_x concentration. This phenomenon occurs because the reaction rate of NO_x with O_3 and other oxidants decreases as NO_x levels rise, a trend particularly pronounced in urban areas with high NO_x concentrations (Laughner and Cohen, 2019). In this study, we aimed to determine the NO_x lifetime in the East Asian environment using WRF-Chem simulations to calculate the NO_x lifetime during daytime. The results are presented in Fig. 6. Daytime was defined as 1–6 UTC (10–15 Korean Standard Time, KST), corresponding to the observation period of the GEMS dataset used in this study. Fig. 6a illustrates the NO_x lifetime averaged over various longitudes across the simulation domain, revealing variations with latitude and altitude. The lifetime generally increases with latitude, consistent with previous findings (Levy II et al., 1999). Notably, the values are substantially higher in the LRT scenario compared to the STG case. At latitudes between 35 and 40°N, encompassing the BTH region, Shandong, and the SMA where high tropospheric NO_2 column concentrations exist, near-surface NO_x lifetimes were approximately 2–3 days in the LRT case, compared to ~1–2 days in the STG case. Additionally, NO_x lifetime exceeded 1 day at altitudes above 850 hPa, where transboundary transport could occur.

The calculated lifetime ranges are slightly higher than those reported by Shah et al. (2020), who estimated a winter residence time of 21–27 h in Eastern China using the GEOS-Chem model. This discrepancy likely arises from differences in study scope, as the previous study included suburban areas and an entire winter season. Satellite-based studies over East Asian megacities suggested NO_x lifetimes of several hours in summer and longer than one day in winter (Liu et al., 2022; Yang et al., 2024), whereas aircraft observations over the United States indicated wintertime lifetimes of ~29 h (Kenagy et al., 2018). Fig. 6b presents calculated lifetimes for the BTH region (longitude 113.45–119.85°E, latitude 36.04–42.63°N), Shandong (longitude 114.84–122.60°E, latitude 34.39–38.27°N), SMA (longitude 126.77–127.18°E, latitude 37.43–37.70°N), and the Yellow Sea (longitude 123.0–126.0°E, latitude 35.0–38.0°N). In the BTH region, NO_x lifetimes of up to 3 days or more were observed in the LRT scenario, suggesting significant potential for pollutant transport to downwind regions. Over the Yellow Sea, NO_2

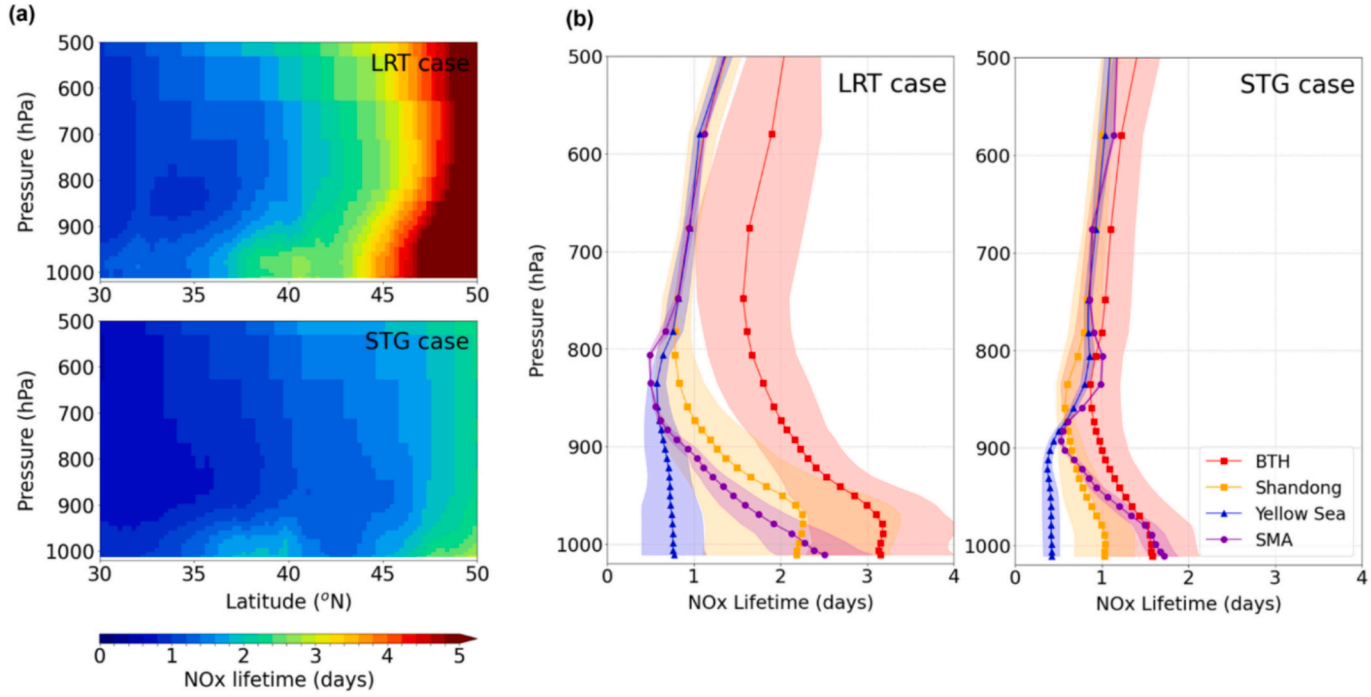

Fig. 6. Vertical distributions of NO_x lifetime during the LRT and STG cases from WRF-Chem simulations, showing domain-wide zonal averages (a) and regional vertical profiles over BTH, Shandong, Yellow Sea, and SMA (b).

persisted in the atmosphere for ~1 day under LRT conditions, further indicating the influence of transboundary transport.

To assess air mass transport speed during spring and winter, when LRT is most prevalent in East Asia, we conducted a trajectory analysis using the FLEXPART-WRF (Fig. 7). Considering WRF-Chem results, the BTH region, which exhibited a relatively long NO_x lifetime, was assumed to be the primary emission source. In addition, receptor-oriented backward trajectory simulations with FLEXPART-WRF for the LRT case indicate that air parcels arriving in Seoul frequently passed over the BTH and Shandong regions, supporting their role as major source areas of NO_2 transport to the Korean Peninsula (Fig. S7). Our simulation indicates that airflows in the lower free troposphere (roughly 1–2 km altitude) are frequently directed eastward. Nevertheless, the direction of air mass movement exhibits notable seasonal variability, alternating among northwesterly, westerly, and southwesterly flows depending on the time of year. Such seasonal shifts align well with the observed surface wind patterns shown in Fig. S4. In particular, during winter and spring—when strong northwesterly to westerly winds are frequently observed—the influence of the East Asian monsoon circulation appears to enhance zonal transport. Under these conditions, air masses originating from the BTH region are often rapidly advected eastward toward the Yellow Sea and the Korean Peninsula, further intensifying west-to-east pollutant transport. Both near the surface and at an altitude of 1.5 km, where LRT primarily occurs, air masses regularly cross the Yellow Sea within 12 h and reach the Korean Peninsula within 24 h during winter and spring. These findings suggest that, despite the relatively short atmospheric lifetime of NO_2 in the lower atmosphere, it can still undergo long-range transport within a short period when westerly winds are strong.

Next, we examined whether NO_x emissions could reach altitudes of 1.5 km. To this end, we analyzed the NO_2 vertical distribution in high-emission regions (35–38°N latitude) using WRF-Chem simulations (Fig. 8). Near-surface NO_2 concentrations exceeded 25 ppbv in the BTH region (115–120°E) and the SMA (127°E), both of which are major emission sources. In the LRT case, vertical mixing was enhanced due to the development of the atmospheric boundary layer and the updraft of a low-pressure system, resulting in well-defined plume structures extending from 950 to 850 hPa (0.5–1.5 km). Notably, these plumes extended from China toward the Korean Peninsula, consistent with the prevailing westerly winds shown by the wind vectors. Consequently, surface NO_2 concentrations over the Yellow Sea were ~5 ppbv higher in the LRT case than in the STG case (Fig. S8). Given that ship emissions account for only a very small fraction of China's total NO_x emissions (Lee et al., 2014), the elevated NO_2 levels in the Yellow Sea suggest a significant contribution from LRT. Further insights are provided in Fig. S9, where lower OH concentrations and higher NO_2/OH ratios in the LRT case indicate prolonged NO_x lifetimes due to reduced oxidation. This trend is particularly evident over the Yellow Sea and in densely populated regions such as BTH and SMA. Additionally, lower yields of alkyl nitrate ($RONO_2$) from $RO_2 + NO$ reactions, compared to nitric acid (HNO_3) formation from $NO_2 + OH$ (Atkinson et al., 1986; Atkinson, 1990, Yeh and Ziemann, 2014), further contribute to NO_x persistence, especially under LRT conditions. These findings underscore the interplay between chemical processes and transport dynamics, supporting the extended NO_x residence time in the LRT case.

4. Conclusions

Our analysis demonstrates that NO_x exhibits a lifetime of 1–3 days in high-emission areas, increasing with altitude, with an average residence time of ~1 day for the same latitude band. Notably, NO_2 can frequently reach altitudes of 1.5 km through slow photochemical processes after surface emissions. Unlike at ground level, where removal mechanisms are more efficient, NO_2 aloft has a residence time exceeding 12 h and can be transported over long distances via fast-moving upper air currents. These results indicate that NO_x lifetime in high-emission regions can be prolonged, facilitating transboundary NO_2 transport at higher altitudes, albeit in smaller amounts than long-lived pollutants. Understanding NO_x as a transboundary pollutant is critical, as transported precursor gases, even in trace amounts, can influence secondary pollutant concentrations along transport pathways and in receptor regions (Lee et al., 2022; Uno et al., 2017; Zhang et al., 2008). This underscores the necessity for

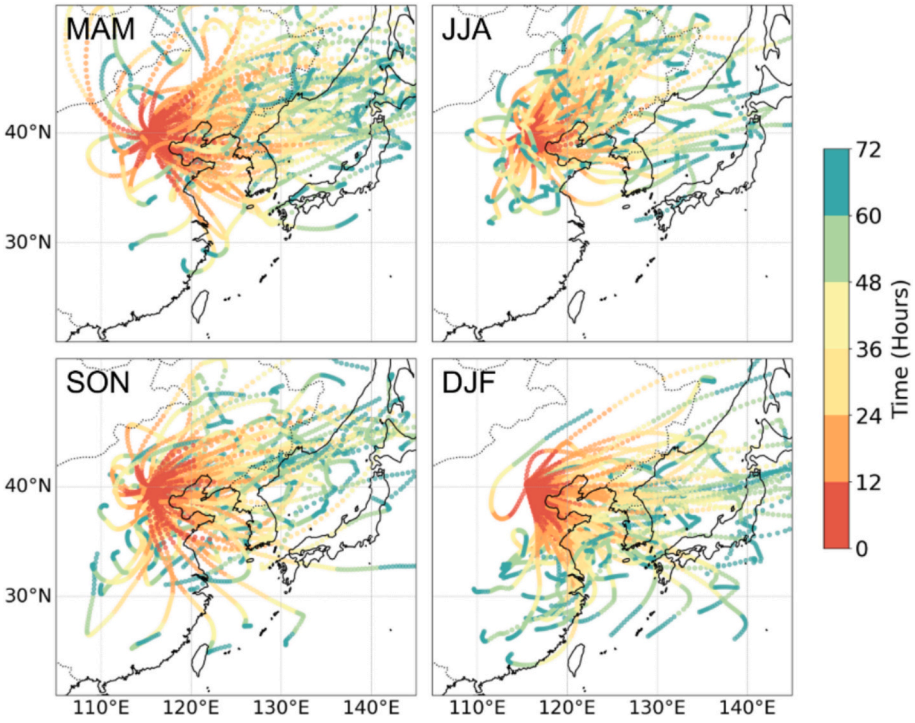

Fig. 7. Seasonal air tracer transport pathways over East Asia from FLEXPART-WRF forward simulations for spring (MAM: March–April–May), summer (JJA: June–July–August), fall (SON: September–October–November) and winter (DJF: December–January–February).

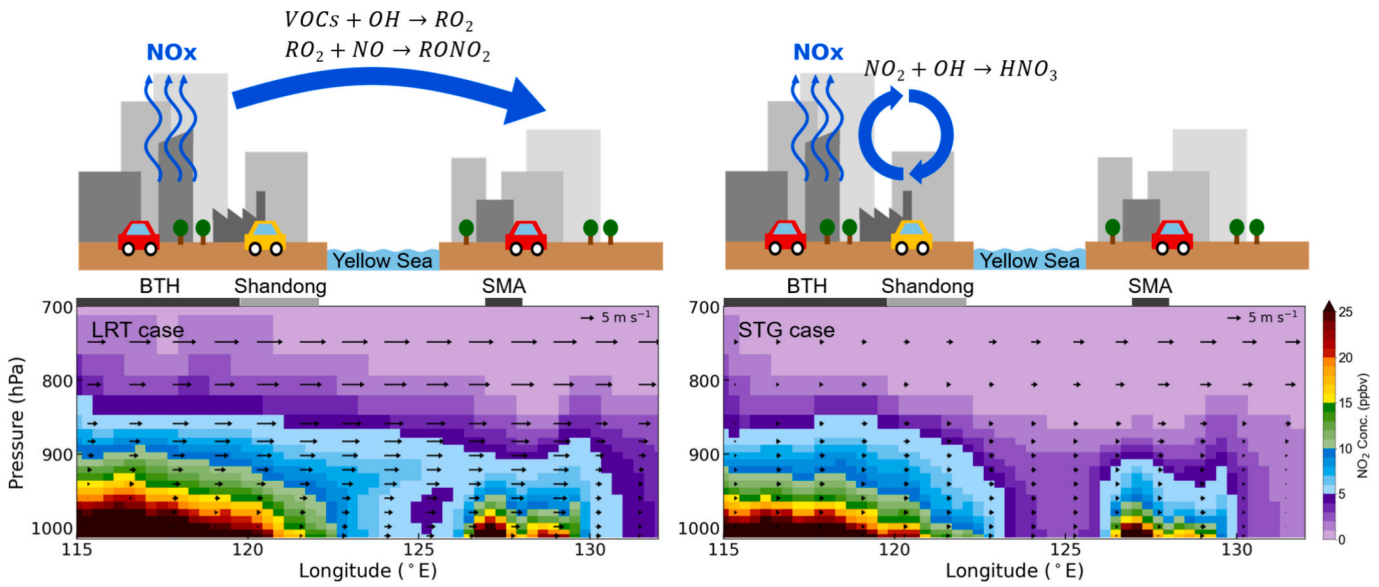

Fig. 8. Conceptual illustrations and WRF-Chem simulated vertical cross-sections of NO_2 for the LRT and STG cases, with wind vectors overlaid to highlight transport pathways.

regional cooperation in air-quality management, including the implementation of enhanced monitoring systems and improved emission control policies to effectively mitigate transboundary pollution.

CRediT authorship contribution statement

Seung-Hee Baek: Writing – review & editing, Writing – original draft, Visualization, Conceptualization. **Hyo-Jung Lee:** Writing – review & editing, Writing – original draft, Visualization, Supervision, Investigation, Conceptualization. **Hyun-Young Jo:** Writing – review & editing. **Cheol-Hee Kim:** Writing – review & editing, Writing – original draft, Supervision. **Min-Jun Park:** Writing – review & editing, Visualization, Investigation. **Jong-Min Kim:** Writing – review & editing, Visualization, Investigation. **Juseon Bak:** Writing – review & editing, Methodology. **Hanlim Lee:** Writing – review & editing, Methodology. **Yeonjin Jung:** Writing – review & editing, Methodology. **Junsung Park:** Writing – review & editing, Methodology, Investigation. **Jung-Hun Woo:** Writing – review & editing, Methodology. **Jinseok Kim:** Writing – review & editing, Investigation. **Rokjin Park:** Writing – review & editing, Methodology. **Lim-Seok Chang:** Writing – review & editing, Methodology. **Chang-Keun Song:** Writing – review & editing, Methodology.

Funding sources

This work was supported by the Basic Science Research Program through the National Research Foundation of Korea (NRF), funded by the Ministry of Education [RS-2020-NR049592] to Seung-Hee Baek, Hyo-Jung Lee, Cheol-Hee Kim, Min-Jun Park, Jong-Min Kim, and Juseon Bak; and by the NRF [RS-2022-NR069425], funded by the Korean Government (MSIT) to Seung-Hee Baek, Hyo-Jung Lee, Min-Jun Park, and Jong-Min Kim.

Declaration of competing interest

The authors declare that they have no known competing financial interests or personal relationships that could have appeared to influence the work reported in this paper.

Acknowledgements

We gratefully acknowledge the National Institute of Environmental Research (NIER) of South Korea for organizing the GMAP2021 and SIJAQ2022 field campaigns, and all participants of the GMAP2021 campaign for their valuable contributions. We also thank the science teams of GEMS and TROPOMI for providing the NO_2 products used in this study.

Appendix A. Supplementary data

Supplementary data to this article can be found online at https://doi.org/10.1016/j.scitotenv.2025.180850.

Data availability

GEMS L2 NO_2 data can be accessed at https://nesc.nier.go.kr/en/html/cntnts/91/static/page.do (National Institute of Environmental Research, NIER, last access: 10 April 2025). The TROPOMI NO_2 data are available at https://documentation.dataspace.copernicus.eu/Data/SentinelMissions/Sentinel5P.html (Copernicus dataspace, last access: 10 April 2025). WRF-Chem codes are available at https://github.com/wrf-model/WRF (last accessed 10 April 2025), and WRF-FLEXPART code can be downloaded at https://www.flexpart.eu/ (last access: 10 April 2025). The SIJAQ campaign dataset including aircraft and in-situ measurements and emission inventory can be obtained by request through the data archive website (https://www.sijaq.org/home, accessed 10 April 2025). The NO_x emission data used in this study are publicly available from the Emissions Database for Global Atmospheric Research (EDGAR) v8.1 Fast Track 2022 (FT2022) Air Pollutant (AP) dataset at: https://edgar.jrc.ec.europa.eu/dataset_ap81. Additional data related to this paper may be requested from the authors. All data needed to evaluate the conclusions in the paper are present in the paper and/or the Supplementary materials.

References

An, X., Yao, B., Li, Y., Li, N., Zhou, L., 2014. Tracking source area of Shangdianzi station using Lagrangian particle dispersion model of FLEXPART. Meteorol. Appl. 21, 466–473. https://doi.org/10.1002/met.1358.

Atkinson, R., 1990. Gas-phase tropospheric chemistry of organic compounds: a review. Atmos. Environ. 24, 1–41. https://doi.org/10.1016/0960-1686(90)90438-S.

Atkinson, R., Aschmann, S.M., Winer, A.M., 1986. Alkyl nitrate formation from the reaction of a series of branched RO_2 radicals with NO as a function of temperature and pressure. J. Atmos. Chem. 5, 91–102. https://doi.org/10.1007/BF00192505.

Bae, K., Song, C.K., Van Roozendael, M., Richter, A., Wagner, T., Merlaud, A., Pinardi, G., Friedrich, M.M., Fayt, C., Dimitropoulou, E., Lange, K., Bosch, T., Zilker, B., Latsch, M., Behrens, L.K., Ziegler, S., Ripperger-Lukosiunaite, S., Kuhn, L., Lauster, B., Reischmann, L., Uhlmannsiek, K., Cede, A., Tiefengraber, M., Gebetsberger, M., Park, R.J., Lee, H., Hong, H., Chang, L.-S., Jeon, S., 2025. Validation of GEMS operational v2.0 total column NO_2 and HCHO during the GMAP/SIJAQ campaign. Sci. Total Environ. 974, 179190. https://doi.org/10.1016/j.scitotenv.2025.179190.

Bassett, M., Seinfeld, J.H., 1983. Atmospheric equilibrium model of sulfate and nitrate aerosols. Atmos. Environ. 17, 2237–2252. https://doi.org/10.1016/0004-6981(83)90221-4.

Beirle, S., Platt, U., Wenig, M., Wagner, T., 2003. Weekly cycle of NO_2 by GOME measurements: a signature of anthropogenic sources. Atmos. Chem. Phys. 3, 2225–2232.

Bovensmann, H., Burrows, J.P., Buchwitz, M., Frerick, J., Noël, S., Rozanov, V.V., Chance, K.V., Goede, A.P.H., 1999. Sciamachy: mission objectives and measurement modes. J. Atmos. Sci. 56, 127–150. https://doi.org/10.5194/acp-3-2225-2003.

Brioude, J., Arnold, D., Stohl, A., Cassiani, M., Morton, D., Seibert, P., Angevine, W., Evan, S., Dingwell, A., Fast, J.D., Easter, R.C., Pisso, I., Burkhart, J., Wotawa, G., 2013. The Lagrangian particle dispersion model FLEXPART-WRF version 3.1. Geosci. Model Dev. 6, 1889–1904. https://doi.org/10.5194/gmd-6-1889-2013.

Callies, J., Corpaccioli, E., Eisinger, M., Hahne, A., Lefebvre, A., 2000. GOME-2 – Metop's second-generation sensor for operational ozone monitoring. ESA Bull. 102, 28–36.

Carmichael, G.R., Calori, G., Hayami, H., Uno, I., Cho, S.Y., Engardt, M., Kim, S.-U., Ichikawa, Y., Ikeda, Y., Woo, J.-H., Ueda, H., Amann, M., 2002. The MICS-Asia study: model intercomparison of long-range transport and sulfur deposition in East Asia. Atmos. Environ. 36, 175–199. https://doi.org/10.1016/S1352-2310(01)00448-4.

Cooper, O.R., Oltmans, S.J., Johnson, B.J., Brioude, J., Angevine, W., Trainer, M., Parrish, D.D., Ryerson, T.R., Pollack, I., Cullis, P.D., Ives, M.A., Tarasick, D.W., Al-Saadi, J., Stajner, I., 2011. Measurement of western U.S. baseline ozone from the surface to the tropopause and assessment of downwind impact regions. J. Geophys. Res. 116, D00V03. https://doi.org/10.1029/2011JD016095.

Cooper, M., Martin, R.V., Padmanabhan, A., Henze, D.K., 2017. Comparing mass balance and adjoint methods for inverse modeling of nitrogen dioxide columns for global nitrogen oxide emissions. J. Geophys. Res. Atmos. 122, 4718–4734. https://doi.org/10.1002/2016JD025985.

Crutzen, P.J., 1970. The influence of nitrogen oxides on the atmospheric ozone content. Q. J. Roy. Meteorol. Soc. 96, 320–325. https://doi.org/10.1007/978-3-319-27460-7_3.

Derwent, R.G., Nodopt, K., 1986. Long-range transport and deposition of acidic nitrogen species in north-west Europe. Nature 324, 356–358. https://doi.org/10.1038/324356a0.

Duncan, B.N., Yoshida, Y., de Foy, B., Lamsal, L.N., Streets, D.G., Lu, Z., Pickering, K.E., Krotkov, N.A., 2013. The observed response of Ozone Monitoring Instrument (OMI) NO_2 columns to NO_x emission controls on power plants in the United States: 2005-2011. Atmos. Environ. 81, 102–111. https://doi.org/10.1016/j.atmosenv.2013.08.068.

Ge, C., Liu, J., Cheng, X., Fang, K., Chen, Z., Chen, Z., Hu, J., Jiang, D., Shen, L., Yang, M., 2022. Impact of regional transport on high ozone episodes in southeast coastal regions of China. Atmos. Pollut. Res. 13, 101497. https://doi.org/10.1016/j.apr.2022.101497.

Granier, C., Brasseur, G.P., 2003. The impact of road traffic on global tropospheric ozone. Geophys. Res. Lett. 30, 1086. https://doi.org/10.1029/2002GL015972.

Grell, G.A., Peckham, S.E., Schmitz, R., McKeen, S.A., Frost, G., Skamarock, W.C., Eder, B., 2005. Fully coupled "online" chemistry within the WRF model. Atmos. Environ. 39, 6957–6975. https://doi.org/10.1016/j.atmosenv.2005.04.027.

Griffin, D., Zhao, X., McLinden, C.A., Boersma, F., Bourassa, A., Dammers, E., Degenstein, D., Eskes, H., Fehr, L., Fioletov, V., Hayden, K., Kharol, S.K., Li, S.-M., Makar, P., Martin, R.V., Mihele, C., Mittermeier, R.L., Krotkov, N., Sneep, M., Lamsal, L.N., Ter Linden, M., van Geffen, J., Veefkind, P., Wolde, M., 2019. High-resolution mapping of nitrogen dioxide with TROPOMI: first results and validation over the Canadian oil sands. Geophys. Res. Lett. 46, 1049–1060. https://doi.org/10.1029/2018GL081095.

Gu, D., Wang, Y., Yin, R., Zhang, Y., Smeltzer, C., 2016. Inverse modelling of NO_x emissions over eastern China: uncertainties due to chemical non-linearity. Atmos. Meas. Tech. 9, 5193–5201. https://doi.org/10.5194/amt-9-5193-2016.

Guerova, G., Bey, I., Attié, J.-L., Martin, R.V., Cui, J., Sprenger, M., 2006. Impact of transatlantic transport episodes on summertime ozone in Europe. Atmos. Chem. Phys. 6, 2057–2072. https://doi.org/10.5194/acp-6-2057-2006.

Itahashi, S., Uno, I., Osada, K., Kamiguchi, Y., Yamamoto, S., Tamura, K., Wang, Z., Kurosaki, Y., Kanaya, Y., 2017. Nitrate transboundary heavy pollution over East Asia in winter. Atmos. Chem. Phys. 17, 3823–3843. https://doi.org/10.5194/acp-17-3823-2017.

Jaeglé, L., Jacob, D.J., Wang, Y., Weinheimer, A.J., Ridley, B.A., Campos, T.L., Sachse, G.W., Hagen, D.E., 1998. Sources and chemistry of NO_x in the upper troposphere over the United States. Geophys. Res. Lett. 25, 1705–1708. https://doi.org/10.1029/97GL03591.

Jaeglé, L., Steinberger, L., Martin, R.V., Chance, K., 2005. Global partitioning of NO_x sources using satellite observations: relative roles of fossil fuel combustion, biomass burning and soil emissions. Faraday Discuss. 130, 407–423. https://doi.org/10.1039/B502128F.

Jung, J., Choi, Y., Souri, A.H., Mousavinezhad, S., Sayeed, A., Lee, K., 2022. The impact of springtime-transported air pollutants on local air quality with satellite-constrained NO_x emission adjustments over East Asia. J. Geophys. Res. Atmos. 127, e2021JD035251. https://doi.org/10.1029/2021JD035251.

Kang, D., Mathur, R., Pouliot, G.A., Gilliam, R.C., Wong, D.C., 2020. Significant ground-level ozone attributed to lightning-induced nitrogen oxides during summertime over the Mountain West States. npj Clim. Atmos. Sci. 3, 6. https://doi.org/10.1038/s41612-020-0108-2.

Karmakar, S., Srinivas, C.V., Rakesh, P.T., Venkatesan, R., Venkatraman, B., 2022. A WRF-FLEXPART simulation study of oil-fire plume dispersion-sensitivity to turbulent diffusion schemes. Meteorol. Atmos. Phys. 134, 32. https://doi.org/10.1007/s00703-022-00866-w.

Kenagy, H.S., Sparks, T.L., Ebben, C.J., Wooldrige, P.J., Lopez-Hilfiker, F.D., Lee, B.H., Thornton, J.A., McDuffie, E.E., Fibiger, D.L., Brown, S.S., Montzka, D.D., Weinheimer, A.J., Schroder, J.C., Campuzano-Jost, P., Day, D.A., Jimenez, J.L., Dibb, J.E., Campos, T., Shah, V., Jaeglé, L., Cohen, R.C., 2018. NO_x lifetime and NO_y partitioning during WINTER. J. Geophys. Res. Atmos. 123, 9813–9827. https://doi.org/10.1029/2018JD028736.

Kim, S.-W., Heckel, A., McKeen, S.A., Frost, G.J., Hsie, E.-Y., Trainer, M.K., Richter, A., Burrows, J.P., Peckham, S.E., Grell, G.A., 2006. Satellite-observed U.S. power plant NO_x emission reductions and their impact on air quality. Geophys. Res. Lett. 33, L22812. https://doi.org/10.1029/2006GL027749.

Kim, J., Jeong, U., Ahn, M.-H., Kim, J.H., Park, R.J., Lee, H., Song, C.H., Choi, Y.-S., Lee, K.-H., Yoo, J.-M., Jeong, M.-J., Park, S.K., Lee, K.-M., Song, C.-K., Kim, S.-W., Kim, Y.J., Kim, S.-W., Kim, M., Go, S., Liu, X., Chance, K., Miller, C.C., Al-Saadi, J., Veihelmann, B., Bhartia, P.K., Torres, O., Abad, G.G., Haffner, D.P., Ko, D.H., Lee, S.H., Woo, J.-H., Chong, H., Park, S.S., Nicks, D., Choi, W.J., Moon, K.-J., Cho, A., Yoon, J., Kim, S.-K., Hong, H., Lee, K., Lee, H., Lee, S., Choi, M., Veefkind, P., Levelt, P.F., Edwards, D.P., Kang, M., Eo, M., Bak, J., Baek, K., Kwon, H.-A., Yang, J., Park, J., Han, K.M., Kim, B.-R., Shin, H.-W., Choi, H., Lee, E., Chong, J., Cha, Y., Koo, J.-H., Irie, H., Hayashida, S., Kasai, Y., Kanaya, Y., Liu, C., Lin, J., Crawford, J.H., Carmichael, G.R., Newchurch, M.J., Lefer, B.L., Herman, J.R., Swap, R.J., Lau, A.K.H., Kurosu, T.P., Jaross, G., Ahlers, B., Dobber, M., McElroy, C.T., Choi, Y., 2020. New era of air quality monitoring from space: geostationary environment monitoring spectrometer (GEMS). Bull. Am. Meteorol. Soc. 101, E1–E22. https://doi.org/10.1175/BAMS-D-18-0013.1.

Kim, C.-H., Jo, H.-Y., Jo, Y.-J., Lee, H.-J., Kim, J.-M., Lee, N.-M., Jeong, S.-Y., Baek, S.-H., Park, M.-J., Chang, L.-S., Lee, J.-J., Song, C.-K., 2023a. Synoptic meteorological conditions and contributing factors to air quality during the SIJAQ campaign. Atmos. Environ. 309, 119939. https://doi.org/10.1016/j.atmosenv.2023.119939.

Kim, S., Kim, J., Hu, H., Jang, M., Lee, J.-B., Hong, S.C., Kim, O., Woo, J.-H., 2023b. Update of the year 2019 modeling emission inventory in China. Asian J. Atmos. Environ. 17, 20. https://doi.org/10.1007/s44273-023-00012-x.

Lamsal, L.N., Martin, R.V., van Donkelaar, A., Celarier, E.A., Bucsela, E.J., Boersma, K.F., Dirksen, R., Luo, C., Wang, Y., 2010. Indirect validation of tropospheric nitrogen dioxide retrieved from the OMI satellite instrument: insight into the seasonal variation of nitrogen oxides at northern midlatitudes. J. Geophys. Res. 115, D05302. https://doi.org/10.1029/2009JD013351.

Lamsal, L.N., Martin, R.V., Padmanabhan, A., van Donkelaar, A., Zhang, Q., Sioris, C.E., Chance, K., Kurosu, T.P., Newchurch, M.J., 2011. Application of satellite observations for timely updates to global anthropogenic NO_x emission inventories. Geophys. Res. Lett. 38, L05810. https://doi.org/10.1029/2010GL046476.

Laughner, J.L., Cohen, R.F., 2019. Direct observation of changing NO_x lifetime in North American cities. Science 366, 723–727. https://doi.org/10.1126/science.aax6832.

Lee, H.-J., Kim, S.-W., Brioude, J., Cooper, O.R., Frost, G.J., Kim, C.-H., Park, R.J., Trainer, M., Woo, J.-H., 2014. Transport of NO_x in East Asia identified by satellite and in situ measurements and Lagrangian particle dispersion model simulations. J. Geophys. Res. Atmos. 119, 2574–2596. https://doi.org/10.1002/2013JD021185.

Lee, H.-J., Jo, H.-Y., Park, S.-Y., Jo, Y.-J., Jeon, W., Ahn, J.-Y., Kim, C.-H., 2019. A case study of the transport/transformation of air pollutants over the Yellow Sea during the MAPS 2015 campaign. J. Geophys. Res. Atmos. 124, 6532–6553. https://doi.org/10.1029/2018JD029751.

Lee, H.-J., Jo, Y.-J., Kim, S., Kim, D., Kim, J.-M., Choi, D., Jo, H.-Y., Bak, J., Park, S.-Y., Jeon, W., Kim, C.-H., 2022. Transboundary aerosol transport process and its impact on aerosol-radiation-cloud feedbacks in springtime over Northeast Asia. Sci. Rep. 12, 4870. https://doi.org/10.1038/s41598-022-08854-1.

Lee, H., Park, J., Jung, Y., Hong, H., 2024. Geostationary Environment Monitoring Spectrometer (GEMS) Algorithm Theoretical Basis Document: NO_2 Retrieval Algorithm. Environmental Satellite Center, National Institute of Environmental Research, Ministry of Environment, Republic of Korea. https://nesc.nier.go.kr/en/html/satellite/doc/doc.do.

Leue, C., Wenig, M., Wagner, T., Klimm, O., Platt, U., Jähne, B., 2001. Quantitative analysis of NO_x emissions from Global Ozone Monitoring Experiment satellite image sequences. J. Geophys. Res. 106, D6. https://doi.org/10.1029/2000JD900572.

Levelt, P.F., Joiner, J., Tamminen, J., Veefkind, J.P., Bhartia, P.K., Zweers, D.C.S., Duncan, B.N., Streets, D.G., Eskes, H., van der A, R., McLinden, C., Fioletov, V., Carn, S., de Laat, J., DeLand, M., Marchenko, S., McPeters, R., Ziemke, J., Fu, D., Liu, X., Pickering, K., Apituley, A., Abad, G.G., Arola, A., Boersma, F., Miller, C.C., Chance, K., de Graaf, M., Hakkarainen, J., Hassinen, S., Ialongo, I., Kleipool, Q., Krotkov, N., Li, C., Lamsal, L., Newman, P., Nowlan, C., Suleiman, R., Tilstra, L.G., Torres, O., Wang, H., Wargan, K., 2018. The Ozone Monitoring Instrument: overview of 14 years in space. Atmos. Chem. Phys. 18, 5699–5745. https://doi.org/10.5194/acp-18-5699-2018.

Levy II, H., Moxim, W.J., Klonecki, A.A., Kasibhatla, P.S., 1999. Simulated tropospheric NO_x: its evaluation, global distribution and individual source contributions. J. Geophys. Res. 104, 26279–26306. https://doi.org/10.1029/1999JD900442.

Li, M., Zhang, Q., Kurokawa, J.-I., Woo, J.-H., He, K., Lu, Z., Ohara, T., Song, Y., Streets, D.G., Carmichael, G.R., Cheng, Y., Hong, C., Huo, H., Jiang, X., Kang, S., Liu, F., Su, H., Zheng, B., 2017. MIX: a mosaic Asian anthropogenic emission inventory under the international collaboration framework of the MICS-Asia and

HTAP. Atmos. Chem. Phys. 17, 935–963. https://doi.org/10.5194/acp-17-935-2017.
Li, Y., Xing, C., Peng, H., Song, Y., Zhang, C., Xue, J., Niu, X., Liu, C., 2023. Long-term observations of NO_2 using GEMS in China: validations and regional transport. Sci. Total Environ. 904, 166762. https://doi.org/10.1016/j.scitotenv.2023.166762.
Liang, Q., Jaeglé, L., Jaffe, D.A., Weiss-Penzias, P., Heckman, A., Snow, J.A., 2004. Long-range transport of Asian pollution to the northeast Pacific: seasonal variations and transport pathways of carbon monoxide. J. Geophys. Res. 109, D23S07. https://doi.org/10.1029/2003JD004402.
Liu, F., Tao, Z., Beirle, S., Joiner, J., Yoshida, Y., Smith, S.J., Knowland, K.E., Wagner, T., 2022. A new method for inferring city emissions and lifetimes of nitrogen oxides from high-resolution nitrogen dioxide observations: a model study. Atmos. Chem. Phys. 22, 1333–1349. https://doi.org/10.5194/acp-22-1333-2022.
Lorente, A., Borsdorff, T., Butz, A., Hasekamp, O., an de Brugh, J., Schneider, A., Wu, L., Hase, F., Kivi, R., Wunch, D., Pollard, D.F., Shiomi, K., Deutscher, N.M., Velazco, V. A., Roehl, C.M., Wennberg, P.O., Warneke, T., Landgraf, J., 2021. Methane retrieved from TROPOMI: improvement of the data product and validation of the first 2 years of measurements. Atmos. Meas. Tech. 14, 665–684. https://doi.org/10.5194/amt-14-665-2021.
Lu, Z., Streets, D.G., 2012. Increase in NO_x emissions from Indian thermal power plants during1996−2010: unit-based inventories and multisatellite observations. Environ. Sci. Technol. 46, 7463–7470. https://doi.org/10.1021/es300831w.
Madala, S., Satyanarayana, A.N.V., Srinivas, C.V., 2015. Simulation of atmospheric dispersion of NO_x over complex terrain region of Ranchi with FLEXPART-WRF by incorporation of improved turbulence intensity relationships. Atmos. Environ. 123, 139–155. https://doi.org/10.1016/j.atmosenv.2015.10.090.
Martin, R.V., Jacob, D.J., Chance, K., Kurosu, T.P., Palmer, P.I., Evans, M.J., 2003. Global inventory of nitrogen oxides emissions constrained by space-based observations of NO_2 columns. J. Geophys. Res. 108, 4537. https://doi.org/10.1029/2003JD003453.
Matandirotya, N.R., Burger, R.P., 2021. Spatiotemporal variability of tropospheric NO_2 over four megacities in southern Africa: implications for transboundary regional air pollution. Environ. Chall. 5, 100271. https://doi.org/10.1016/j.envc.2021.100271.
Oak, Y.J., Jacob, D.J., Balasus, N., Yang, L.H., Chong, H., Park, J., Lee, H., Lee, G.T., Ha, E.S., Park, R.J., Kwon, H.-A., Kim, J., 2024. A bias-corrected GEMS geostationary satellite product for nitrogen dioxide using machine learning to enforce consistency with the TROPOMI satellite instrument. Atmos. Meas. Tech. 17, 5147–5159. https://doi.org/10.5194/amt-17-5147-2024.
Parrish, D.D., Dunlea, E.J., Atlas, E.L., Schauffler, S., Donnelly, S., Stroud, V., Goldstein, A.H., Millet, D.B., McKay, M., Jaffe, D.A., Price, H.U., Hess, P.G., Flocke, F., Roberts, J.M., 2004. Changes in the photochemical environment of the temperate North Pacific troposphere in response to increased Asian emissions. J. Geophys. Res. 109, D23S18. https://doi.org/10.1029/2004JD004978.
Platt, U., Stutz, J., 2008. Differential Optical Absorption Spectroscopy: Principles and Applications, 1st ed. Springer, Berlin.
Qu, Y., An, J., He, Y., Zheng, J., 2016. An overview of emissions of SO_2 and NO_x and the long-range transport of oxidized sulfur and nitrogen pollutants in East Asia. J. Environ. Sci. 44, 13–25. https://doi.org/10.1016/j.jes.2015.08.028.
Richter, A., Burrows, J.P., Nüß, H., Granier, C., Niemeier, U., 2005. Increase in tropospheric nitrogen dioxide over China observed from space. Nature 437, 129–132. https://doi.org/10.1038/nature04092.
Schaub, D., Weiss, A.K., Kaiser, J.W., Petritoli, A., Richter, A., Buchmann, B., Burrows, J. P., 2005. A transboundary transport episode of nitrogen dioxide as observed from GOME and its impact in the Alpine region. Atmos. Chem. Phys. 5, 23–37. https://doi.org/10.5194/acp-5-23-2005.
Seo, S., Kim, S.-W., Kim, K.-M., Richter, A., Lange, K., Burrows, J.P., Park, J., Hong, H., Lee, H., Jeong, U., Woo, J.-H., Kim, J., 2025. Diurnal variations of NO_2 tropospheric vertical column density over the Seoul metropolitan area from the Geostationary Environment Monitoring Spectrometer (GEMS): seasonal differences and the influence of the a priori NO_2 profile. Atmos. Meas. Tech. 18, 115–128. https://doi.org/10.5194/amt-18-115-2025.
Shah, V., Jacob, D.J., Li, K., Silvern, R.F., Zhai, S., Liu, M., Lin, J., Zhang, Q., 2020. Effect of changing NO_x lifetime on the seasonality and long-term trends of satellite-observed tropospheric NO_2 columns over China. Atmos. Chem. Phys. 20, 1483–1495. https://doi.org/10.5194/acp-20-1483-2020.
Skamarock, W.C., Klemp, J.B., Dudhia, J., Gill, D.O., Barker, D., Duda, M.G., Huang, X., Wang, W., Powers, J.G., 2008. A description of the advanced research WRF version 3. In: NCAR Technical Note NCAR/TN-475+STR. National Center for Atmospheric Research, Boulder, CO, USA. https://doi.org/10.5065/D68S4MVH.
Stavrakou, T., Müller, J.-F., Boersma, K.F., De Smedt, I., Van der A, R.J., 2008. Assessing the distribution and growth rates of NO_x emission sources by inverting a 10-year record of NO_2 satellite columns. Geophys. Res. Lett. 35, L10801. https://doi.org/10.1029/2008GL033521.
Stohl, A., Eckhardt, S., Forster, C., James, P., Spichtinger, N., 2002. On the pathways and timescales of intercontinental air pollution transport. J. Geophys. Res. 107, 4684. https://doi.org/10.1029/2001JD001396.
Stohl, A., Prata, A.J., Eckhardt, S., Clarisse, L., Durant, A., Henne, S., Kristiansen, N.I., Minikin, A., Schumann, U., Seibert, P., Stebel, K., Thomas, H.E., Thorsteinsson, T., Tørseth, K., Weinzierl, B., 2011. Determination of time- and height-resolved volcanic ash emissions and their use for quantitative ash dispersion modeling: the 2010 Eyjafjallajökull eruption. Atmos. Chem. Phys. 11, 4333–4351. https://doi.org/10.5194/acp-11-4333-2011.
Thomas, M.A., Devasthale, A., 2017. Typical meteorological conditions associated with extreme nitrogen dioxide (NO_2) pollution events over Scandinavia. Atmos. Chem. Phys. 17, 12071–12080. https://doi.org/10.5194/acp-17-12071-2017.
Thompson, A.M., Stauffer, R.M., Boyle, T.P., Kollonige, D.E., Miyazaki, K., Tzortziou, M., Herman, J.R., Abuhassan, N., Jordan, C.E., Lamb, B.T., 2019. Comparison of near-surface NO_2 pollution with Pandora total column NO_2 during the Korea-United States Ocean Color (KORUS OC) campaign. J. Geophys. Res. Atmos. 124, 13560–13575. https://doi.org/10.1029/2019JD030765.
Uno, I., Osada, K., Yumimoto, K., Wang, Z., Itahashi, S., Pan, X., Hara, Y., Yamamoto, S., Nishizawa, T., 2017. Importance of long-range nitrate transport based on long-term observation and modeling of dust and pollutants over East Asia. Aerosol Air Qual. Res. 17, 3052–3064. https://doi.org/10.4209/aaqr.2016.11.0494.
Valin, L.C., Russell, A.R., Hudman, R.C., Cohen, R.C., 2011. Effects of model resolution on the interpretation of satellite NO_2 observations. Atmos. Chem. Phys. 11, 11647–11655. https://doi.org/10.5194/acp-11-11647-2011.
van der A, R.J., Peters, D.H.M.U., Eskes, H., Boersma, K.F., Van Roozendael, M., De Smedt, I., Kelder, H.M., 2006. Detection of the trend and seasonal variation in tropospheric NO_2 over China. J. Geophys. Res. 111, D12317. https://doi.org/10.1029/2005JD006594.
van der A, R.J., Eskes, H.J., Boersma, K.F., van Noije, T.P.C., Van Roozendael, M., De Smedt, I., Peters, D.H.M.U., Meijer, E.W., 2008. Trends, seasonal variability and dominant NO_x source derived from a ten year record of NO_2 measured from space. J. Geophys. Res. 113, D04302. https://doi.org/10.1029/2007JD009021.
van Geffen, J.H.G.M., Eskes, H.J., Boersma, K.F., Maasakkers, J.D., Veefkind, J.P., 2019. TROPOMI ATBD of the Total and Tropospheric NO_2 Data Products. S5P-KNMI-L2-0005-RP. Royal Netherlands Meteorological Institute, De Bilt, Netherlands. https://sentinel.esa.int/documents/247904/2476257/Sentinel-5P-TROPOMI-ATBD-NO2-data-products.pdf.
Veefkind, J.P., Aben, I., McMullan, K., Förster, H., de Vries, J., Otter, G., Claas, J., Eskes, H.J., de Haan, J.F., Kleipool, Q., van Weele, M., Hasekamp, O., Hoogeveen, R., Landgraf, J., Snel, R., Tol, P., Ingmann, P., Voors, R., Kruizinga, B., Vink, R., Visser, H., Levelt, P.F., 2012. TROPOMI on the ESA sentinel-5 precursor: a GMES mission for global observations of the atmospheric composition for climate, air quality and ozone layer applications. Remote Sens. Environ. 120, 70–83. https://doi.org/10.1016/j.rse.2011.09.027.
Wang, S., Xing, J., Jang, C., Zhu, Y., Fu, J.S., Hao, J., 2011. Impact assessment of ammonia emissions on inorganic aerosols in East China using response surface modeling technique. Environ. Sci. Technol. 45, 9293–9300. https://doi.org/10.1021/es2022347.
Wenig, M., Spichtinger, N., Stohl, A., Held, G., Beirle, S., Wagner, T., Jähne, B., Platt, U., 2003. Intercontinental transport of nitrogen oxide pollution plumes. Atmos. Chem. Phys. 3, 387–393. https://doi.org/10.5194/acp-3-387-2003.
Woo, J.-H., Kim, Y., Kim, H.-K., Choi, K.-C., Eum, J.-H., Lee, J.-B., Lim, J.-H., Kim, J., Seong, M., 2020. Development of the CREATE inventory in support of integrated climate and air quality modeling for Asia. Sustainability 12, 7930. https://doi.org/10.3390/su12197930.
Yang, L.H., Jacob, D.J., Dang, R., Oak, Y.J., Lin, H., Kim, J., Zhai, S., Colombi, N.K., Pendergrass, D.C., Beaudry, E., Shah, V., Feng, X., Yantosca, R.M., Chong, H., Park, J., Lee, H., Lee, W.-J., Kim, S., Kim, E., Travis, K.R., Crawford, J.H., Liao, H., 2024. Interpreting Geostationary Environment Monitoring Spectrometer (GEMS) geostationary satellite observations of the diurnal variation in nitrogen dioxide (NO_2) over East Asia. Atmos. Chem. Phys. 24, 7027–7039. https://doi.org/10.5194/acp-24-7027-2024.
Yeh, G.K., Ziemann, P.J., 2014. Alkyl nitrate formation from the reactions of C_8-C_{14} *n*-alkanes with OH radicals in the presence of NO_x: measured yields with essential corrections for gas-wall partitioning. J. Phys. Chem. A 118, 8147–8157. https://doi.org/10.1021/jp500631v.
Zhang, Q., Streets, D.G., He, K., Wang, Y., Richter, A., Burrows, J.P., Uno, I., Jang, C.J., Chen, D., Yao, Z., Lei, Y., 2007. NO_x emission trends for China, 1995-2004: the view from the ground and the view from space. J. Geophys. Res. 112, D22306. https://doi.org/10.1029/2007JD008684.
Zhang, L., Jacob, D.J., Boersma, K.F., Jaffe, D.A., Olson, J.R., Bowman, K.W., Worden, J. R., Thompson, A.M., Avery, M.A., Cohen, R.C., Dibb, J.E., Flock, F.M., Fuelberg, H. E., Huey, L.G., McMillan, W.W., Singh, H.B., Weinheimer, A.J., 2008. Transpacific transport of ozone pollution and the effect of recent Asian emission increases on air quality in North America: an integrated analysis using satellite, aircraft, ozonesonde, and surface observations. Atmos. Chem. Phys. 8, 6117–6136. https://doi.org/10.5194/acp-8-6117-2008.
Zhang, Q., Streets, D.G., Carmichael, G.R., He, K.B., Huo, H., Kannari, A., Klimont, Z., Park, I.S., Reddy, S., Fu, J.S., Chen, D., Duan, L., Lei, Y., Wang, L.T., Yao, Z.L., 2009. Asian emissions in 2006 for the NASA INTEX-B mission. Atmos. Chem. Phys. 9, 5131–5153. https://doi.org/10.5194/acp-9-5131-2009.